IDENTIFICATION OF MAIN-SEQUENCE STARS WITH MID-INFRARED EXCESSES USING GLIMPSE: β PICTORIS ANALOGS?

B. Uzpen,[1] H. A. Kobulnicky,[1] K. A. G. Olsen,[2] D. P. Clemens,[3] T. L. Laurance,[1] M. R. Meade,[4] B. L. Babler,[4]
R. Indebetouw,[4] B. A. Whitney,[5] C. Watson,[4] M. G. Wolfire,[6] M. J. Wolff,[5] R. A. Benjamin,[7] T. M. Bania,[3]
M. Cohen,[8] K. E. Devine,[4] J. M. Dickey,[9] F. Heitsch,[10] J. M. Jackson,[3] A. P. Marston,[11] J. S. Mathis,[4]
E. P. Mercer,[3] J. R. Stauffer,[12] S. R. Stolovy,[12] D. E. Backman,[13] AND E. Churchwell[4]

ABSTRACT

Spitzer IRAC 3.6–8 μm photometry obtained as part of the GLIMPSE survey has revealed mid-infrared excesses for 33 field stars with known spectral types in a $1.2 \deg^2$ field centered on the southern Galactic H II region RCW 49. These stars comprise a subset of 184 stars with known spectral classification, most of which were preselected to have unusually red IR colors. We propose that the mid-IR excesses are caused by circumstellar dust disks that are either very late remnants of stellar formation or debris disks generated by planet formation. Of these 33 stars, 29 appear to be main-sequence stars on the basis of optical spectral classifications. Five of the 29 main-sequence stars are O or B stars with excesses that can be plausibly explained by thermal bremsstrahlung emission, and four are post–main-sequence stars. The lone O star is an O4 V((f)) at a spectrophotometric distance of 3233^{+540}_{-535} pc and may be the earliest member of the Westerlund 2 cluster. Of the remaining 24 main-sequence stars, 18 have spectral energy distributions that are consistent with hot dusty debris disks, a possible signature of planet formation. Modeling the excesses as blackbodies demonstrates that the blackbody components have fractional bolometric disk-to-star luminosity ratios, L_{IR}/L_*, ranging from 10^{-3} to 10^{-2} with temperatures ranging from 220 to 820 K. The inferred temperatures are more consistent with asteroid belts than with the cooler temperatures expected for Kuiper belts. Mid-IR excesses are found in all spectral types from late B to early K.

Subject headings: circumstellar matter — open clusters and associations: individual (Westerlund 2) — planetary systems: formation

1. INTRODUCTION

Infrared Astronomical Satellite (*IRAS*) observations of Vega detected an infrared excess above the photospheric level, suggesting the presence of circumstellar material (Aumann et al. 1984). Follow-up observations found infrared excesses around other main-sequence stars, including β Pictoris. Coronographic imaging identified a resolved dusty disk around β Pictoris as the cause of the infrared excess (Smith & Terrile 1984). β Pictoris's

[1] Department of Physics and Astronomy, University of Wyoming, Department 3905, Laramie, WY 82071.

[2] Visiting Astronomer, Cerro Tololo Inter-American Observatory, National Optical Astronomy Observatory, which is operated by the Association of Universities for Research in Astronomy, under contract with the National Science Foundation; and National Optical Astronomy Observatory, Casilla 603, La Serena, Chile.

[3] Institute for Astrophysical Research, Boston University, 725 Commonwealth Avenue, Boston, MA 02215.

[4] Department of Astronomy, University of Wisconsin, 475 North Charter Street, Madison, WI 53706.

[5] Space Science Institute, 4750 Walnut Street, Suite 205, Boulder, CO 80301.

[6] Department of Astronomy, University of Maryland, College Park, MD 20742-2421.

[7] Physics Department, University of Wisconsin, 800 West Main Street, Whitewater, WI 53190.

[8] Radio Astronomy Laboratory, University of California, 601 Campbell Hall, Berkeley, CA 94720.

[9] Department of Astronomy, University of Minnesota, 116 Church Street Southeast, Minneapolis, MN 55455.

[10] Institute for Astronomy and Astrophysics, University of Munich, Scheinerstrasse 1, 81679 Munich, Germany.

[11] ESTEC/SCI-SA, Postbus 299, 2200 AG Noordwijk, Netherlands.

[12] *Spitzer* Science Center, Caltech, MS 314-6, Pasadena, CA 91125.

[13] SOFIA, MS 211-3, NASA-Ames Research Center, Moffett Field, CA 94035-1000.

disk is a prototype for a young but nearly complete planetary system. Identification of this disk was the first observational evidence of planetary systems outside our own. Many nearby stars have been investigated using *IRAS* and the *Infrared Space Observatory* (*ISO*) to search for far-IR photospheric excesses, and a large number have been found (Lagrange et al. 2000; Backman & Paresce 1993 and references therein). Due to the large beam size of *IRAS*, far-IR observations of nearby stars such as β Pictoris, ε Eradani, Fomalhaut, and others have resulted in follow-up higher resolution ground-based mid-IR observations. These observations resolved their disks and probed their compositions (Lagrange et al. 2000). Stars with far-IR excesses, such as ε Eradani, may even harbor planets (Hatzes et al. 2000).

Only a few main-sequence stars with mid-IR but no near-IR excesses have been detected. Aumann & Probst (1991) investigated nearby main-sequence stars using 12 μm measurements from *IRAS*, but of the 548 stars investigated, only 13 had colors unusual enough to warrant further investigation. Follow-up ground-based observations were conducted on seven stars at 10 μm to determine whether the excess originated from the star. Only β Pictoris and ζ Leporis exhibited mid-IR excesses (Aumann & Probst 1991). Chen & Jura (2001) measured a temperature of 370 K for the mid-IR excess in ζ Leporis and suggested that it is due to a massive asteroid belt. The excess in ζ Leporis originates at small radii, less than 6 AU, and not at large radii, ≥40 AU, unlike other stars, such as β Pictoris, that have large disks extending hundreds of AU (Chen & Jura 2001). Stars with higher disk temperatures have dust that is closer to the star, and the excess may be more analogous to the warm temperatures of asteroid belts than to the ~100 K dust of Kuiper Belts.

Evidence for planets around nearby stars is now overwhelming, with over 120 planets in 100+ planetary systems,[14] most found using high-resolution stellar spectroscopy capable of detecting Doppler shifts in the parent star. However, the process or processes by which these planets form is still unknown. Planetesimals may originate in circumstellar disks, formed as a by-product of star formation. The evolutionary sequence of both inner and outer circumstellar disks from pre–main sequence to main sequence is not well understood (Meyer & Beckwith 2000). Lack of observational evidence of an evolutionary disk sequence is a major hindrance in the understanding of planetary formation. The reason for this lack of evidence is that only the nearest stars have been probed for circumstellar disks, and a relatively small number of stars with disks have been identified. It is estimated that at least 15% of nearby A–K main-sequence stars have dusty debris disks that were detectable to *IRAS* and *ISO* sensitivities in the far-IR (Lagrange et al. 2000; Backman & Paresce 1993).

The *Spitzer Space Telescope* (*Spitzer*) Legacy program includes two surveys investigating the formation of stars and the processes leading to the formation of solar systems: the "Cores to Disks" (C2D; Evans et al. 2003) and "Formation and Evolution of Planetary Systems" (FEPS; Meyer et al. 2001) projects. Data from these programs will cover a large portion of the spectral energy distribution (SED) of stars, as well as provide insight into the structure and evolution of circumstellar disks. The focus of the C2D project is on stellar cores and very young stars with ages up to ~10 Myr. The FEPS project focuses on older solar analogs, 3 Myr to 3 Gyr, to determine disk composition and characterize their evolutionary stages. The FEPS and C2D projects are, however, narrowly focused in spatial coverage, with C2D covering ~20 deg^2 and FEPS focusing on ~350 individual stars out to ~200 pc.

In this study, we have utilized a subset of the Galactic Legacy Infrared Mid-Plane Survey Extraordinaire (GLIMPSE; Benjamin et al. 2003) database to try to identify main-sequence stars with mid-IR excesses. Given the sensitivity of *Spitzer*, we expect to be able to detect unreddened A stars to ~4 kpc, F stars to ~2 kpc, G stars to ~1.3 kpc, and K stars to ~1 kpc. Given these distances, we will survey a much larger volume of space for stars exhibiting mid-IR excesses than any previous study.

Optical spectra were obtained to determine whether near and mid-IR colors could indicate a spectral sequence. In this paper we present results of a survey of the GLIMPSE Observation Strategy Validation (OSV) region in the vicinity of the southern Galactic star-forming region RCW 49, where the Westerlund 2 open cluster is centered (Churchwell et al. 2004). We obtained optical spectroscopy for a sample of stars with red or unusual near and mid-IR colors. We combine optical photometry and spectroscopy with near and mid-IR photometry to model the SEDs of the stars. Once a star is shown to exhibit a mid-IR excess, we model the excess as a single blackbody to gain some insight into its basic properties. In § 2 we discuss the photometry obtained with GLIMPSE and the method of classification of spectral types. In § 3 we discuss how stars with mid-IR excesses were identified, and in § 4 we compare the stars with mid-IR excesses to the prototype debris disk system, β Pictoris. In § 5 we discuss the lone O4 V((f)) star that exhibits a mid-IR excess and its implications for the age and distance of Westerlund 2. This is a preliminary investigation to determine whether warm debris disks can be detected with the GLIMPSE survey in the mid-IR.

2. DATA

2.1. *GLIMPSE Photometry*

The GLIMPSE project is one of six *Spitzer* Legacy Programs. GLIMPSE mapped the Galactic plane in four infrared array camera (IRAC; Fazio et al. 2004) band passes, [3.6], [4.5], [5.8], and [8.0] μm from $|l| = 10°–65°$ and $|b| < 1°$ (Benjamin et al. 2003). This survey has generated a point-source catalog of 3×10^7 objects. The GLIMPSE program is the largest, most sensitive, mid-IR survey to date. The GLIMPSE program mapped RCW 49 as part of the OSV (Churchwell et al. 2004). This region was mapped 10 times with 1.2 s exposures by IRAC and is therefore the deepest region surveyed by the GLIMPSE program. A total of 38,734 mid-IR catalog sources were found in the OSV. To be included in the point-source catalog, a source must have a signal-to-noise ratio of greater than 5:1 with at least two detections in one band and at least one detection in an adjacent band with fluxes greater than 0.6, 0.6, 2, and 10 mJy (in bands 1 through 4, respectively). The other two bands need only have a signal-to-noise ratio of greater than 3:1. See the GLIMPSE data document,[15] Mercer et al. (2004), Churchwell et al. (2004), Whitney et al. (2004), or Indebetouw et al. (2005) for further descriptions.

2.2. *Spectra*

We obtained optical spectroscopy of 220 stars in the GLIMPSE OSV field surrounding RCW 49 using the Hydra instrument on the CTIO 4 m on the night of 2004 March 1 using three fiber configurations. The instrument configuration used the large 2″ fibers and the KGPL1 grating, which provides a dispersion of 0.6 Å pixel^{-1}, a spectral resolution of 4.2 Å, and wavelength coverage of ~2400 Å from ~3600 to 6000 Å. This wavelength regime covers the majority of the hydrogen Balmer series, Ca H and K, as well as many metal lines, which are necessary for luminosity and temperature classification. Total exposure times were 20 minutes for the first fiber configuration and 60 minutes for the second and third fiber configurations. Sky conditions were photometric.

We selected target stars on the basis of preliminary GLIMPSE photometry in all four IRAC bandpasses, along with Two Mass All Sky Survey (2MASS)[16] and Guide Star Catalog 2.2 (GSC)[17] photometry. The stars were selected using optical brightness and infrared colors. The stars in the first fiber configuration consisted of *High-Precision Parallax-Collecting Satellite* (*Hipparcos*) and Tycho Catalog stars and bright GSC stars with $V \leq 13$. Bright stars with 2MASS/IRAC colors indicative of possible IR excesses were also placed in the first two fiber fields. We selected as stars with colors indicating an IR-excess or extreme
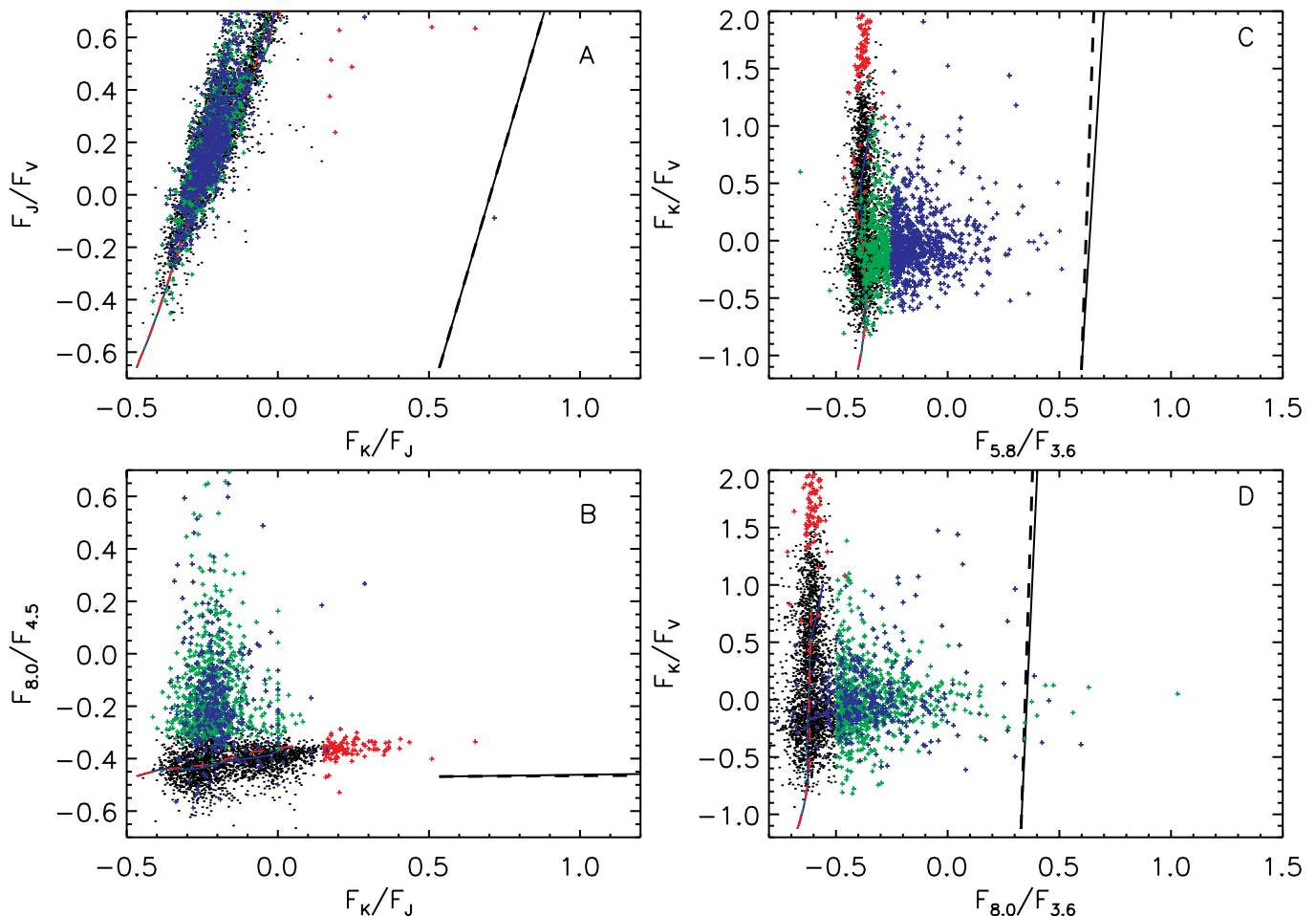

Fig. 1.—Color-color plots of cataloged point sources in the GLIMPSE OSV region (Westerlund 2 region). The black lines are the extinction vectors of Li & Draine (2001). The dashed vectors are the extinction laws of Indebetouw et al. (2005) in the mid-IR. Both sets of extinction lines represent $A_V = 10$ and are offset from the stellar loci for clarity. The green plus signs are $\log F_{8.0}/F_{3.6} \geq -0.5$ (criterion 1), the red plus signs are $\log F_K/F_J \geq 0.15$ (criterion 2), and the blue plus signs are $\log F_{5.8}/F_{3.6} \geq -0.25$ (criterion 3).

reddening those that satisfied one or more of the following criteria: flux ratios $\log F_{8.0}/F_{3.6} \geq -0.5$ (criterion 1), $\log F_K/F_J \geq 0.15$ (criterion 2), or $\log F_{5.8}/F_{3.6} \geq -0.25$ (criterion 3). We chose these criteria to sample a representative distribution of objects with unusual infrared colors. Criterion 1 sources comprise the reddest ∼15% of sources with visual counterparts, criterion 2 sources comprise the reddest ∼2%, and criterion 3 comprise the reddest ∼13%. Color-color plots of the data set used in selecting stars are shown in Figure 1. Stars that met criterion 1, 2, and 3 are plotted as green, red, and blue plus signs, respectively. Figure 1 gives a representative view of the color-color space occupied by the stars meeting one or more of the three criteria.

The second fiber field consisted of stars with GSC photometry and IR colors satisfying one or more of the three color criteria. The third fiber field consisted of stars meeting one or more of the color criteria, but some stars did not have GSC V-band counterparts, allowing for the inclusion of extremely red stars.

A total of 164 new stellar classifications resulted from these observations. The stars were classified by eye using comparison spectra (Yamashita et al. 1976) to within two comparison temperature classes of the atlas. There were 56 stars too faint or featureless for classification. Protostars may comprise a significant fraction of these unclassified objects because they have high extinctions and are optically faint. There are ∼50 stars in

the OSV that had previous spectral classifications in the literature, but most of them were saturated in GLIMPSE, so their mid-IR colors are unreliable and are not included in this investigation. We were able to use 20 stars that had suitable GLIMPSE colors and were previously classified in the literature.

3. ANALYSIS

The positions of 38,734 GLIMPSE Point Source Catalog objects in the OSV were matched against the positions of 2MASS Point Source Catalog objects using the GLIMPSE data reduction pipeline. We then matched the Guide Stars with the GLIMPSE objects to produce V, J, H, K, [3.6], [4.5], [5.8], and [8.0] photometry for the 184 spectrally classified stars, although some objects lack photometry at one or more of the eight bandpasses. The GSC V-band photometry was extracted from photometric plates, and most stars have V-band uncertainties of ∼0.4 mag (see the GSC documentation for more information).

The eight photometric data points were fit with Kurucz ATLAS 9 models using temperatures and effective gravities corresponding to the nearest spectral type (Kurucz 1993). Since all of the stars lie within the solar circle, we adopt the solar metallicity models. The Kurucz model surface fluxes were scaled by a factor, X, so that the model K-band fluxes matched the observed K-band 2MASS photometry. This scale factor represents $X = R^2/D^2$, the ratio of the stellar radius squared over the

distance to the star squared. Adopting stellar radii appropriate for the observed spectral types (De Jager & Nieuwenhuijzen 1987; Schmidt-Kaler 1982; Johnson 1966), we calculated a spectrophotometric distance to each star. These distances and their uncertainties, estimated by taking into account the K-band photometric errors added in quadrature with an additional 15% uncertainty in the stellar radii, are listed in the tables. The K-band measurements were used as the basis for the distance computation because the effects of extinction are nearly negligible at 2.2 μm for most of our stars. Our derived A_V are all <1.5 mag, implying $A_K < 0.15$ mag. The model atmospheres were reddened with variable amounts of extinction using the Li & Draine (2001) extinction curve, except in the mid-IR ($\lambda > 3$ μm) where the GLIMPSE extinction results were used (Indebetouw et al. 2005). Distance and extinction were fit iteratively as free parameters covering a grid of all reasonable values. The best-fit parameters for each star are determined by the minimum of the χ^2 statistic. Modeling the star with the next earlier or later spectral type model available in the Kurucz library (i.e., an A3 with an A0 or an A5) produced very similar reduced χ^2 values. This allows small errors in classification to yield similar results. This also provides a check on classification. If a star is grossly misclassified, the fit is poor and the classification is double-checked.

We performed a trial fitting procedure in which the effective temperatures and gravities of the stellar models were allowed to vary as free parameters (i.e., the program searched through the entire library of Kurucz models to find a best fit). In nearly all cases, this method produced fits with lower χ^2, but this approach frequently converged on temperature and gravity combinations that were grossly inconsistent with the observed spectral types. We found that there was often a degeneracy between the amount of extinction and the effective temperature, such that models with high temperatures and low extinctions yielded similar fits as models with low temperatures and high extinctions. We therefore chose to fix the effective temperatures and gravities of the models at values appropriate to the classified spectral type.

Our data set consisted of 184 main-sequence, giant, and supergiant stars with spectral types in the OSV region. This sample included 20 stars with known spectral types from the literature that had reliable GLIMPSE photometry as well as the 164 sources for which we obtained new classifications. We calculated $(K - 8)$ color excesses, $E(K - 8)$, by taking the differences between the Kurucz photospheric model and the photometric $(K - 8)$. We chose the $(K - 8)$ color because main-sequence stars should exhibit minimal color differences for these wavelengths. This method is similar to the method used by Aumann & Probst (1991), in which $K - 12$ from *IRAS* was used to identify warm disk candidates.

Figure 2 shows the $E(K - 8)$ distribution of stars with $(K - 8)$ colors. The distribution shows a peak with a mean near $E(K - 8) = 0.08$ and a long tail toward larger excesses. The majority of stars, 110, have $E(K - 8)$ between -0.2 and 0.35, with a mean of 0.08 and a dispersion of 0.09. There were 33 stars with excesses larger than 3 times the dispersion of the main group, i.e., with an $E(K - 8) \geq 0.35$. Of these 33 stars with possible mid-IR excesses, three did not have measurements at [5.8], and three of the stars had photometric uncertainties placing them within one standard deviation from an $E(K - 8)$ of 0.35. In order to place a higher reliability on our detections we required that the stars have all four IRAC measurements and an $E(K - 8) \geq 0.35 + 1$ σ. Table 1 gives the colors and uncertainties for the 18 main-sequence stars satisfying the above criteria, along with their spectral types and color uncertainties. Hereafter, we refer to this group of stars as the "G18" sample. Table 2 contains the
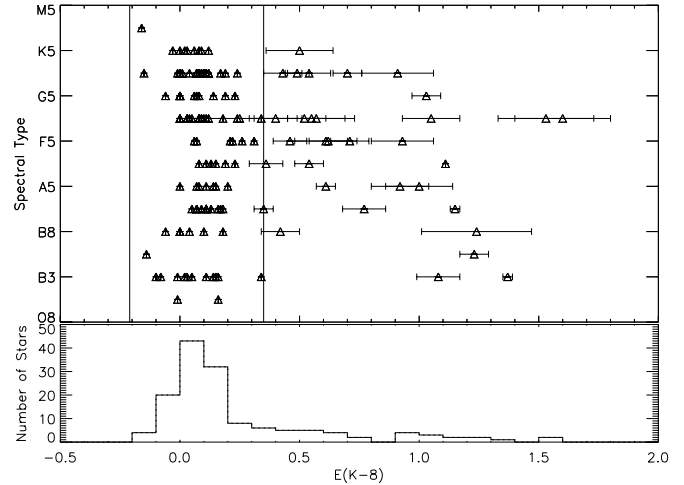

Fig. 2.—Kurucz model spectral class vs. the $(K - 8)$ color excess. The majority of stars have no significant $(K - 8)$ excess and cluster between -0.21 and 0.35 (denoted by the vertical bars), while 33 stars have an excess greater than 0.35 mag. The vertical lines denote the 3 σ dispersion from the mean of the 110 stars without excesses. The distribution shows that there is a long tail with excesses exhibited by stars of all spectral classes.

stars that had an excess greater than 0.35 but did not meet all of our criteria for inclusion in Table 1. Table 2 include stars that did not have all four IRAC measurements, or stars of early spectral type where the excess could be explained by thermal bremsstrahlung emission (see 3.1).

Figure 3 shows color-color plots of the stars with mid-IR excesses. Panel *a* shows that the stars with a $(K - 8)$ excess exhibit typical colors for the J, H, and K near-IR, but in panel *d* they show a significant deviation from the main-sequence that cannot be explained by reddening. Stars that could not be classified because of an insufficient signal-to-noise ratio in the optical spectra are shown only in panel *b* because almost all of these stars were in field 3 and did not have a *V*-band measurement. Triangles denote stars with a mid-IR excess that did not have *V*-band measurements. Nearly all of the unidentified stars have F_K/F_J much redder than the stars exhibiting mid-IR excesses. These stars are likely to be highly extinguished and could be protostars.

3.1. *The Mid-IR Excesses*

We analyzed the SEDs of the 23 stars meeting the above "excess" criteria to determine whether phenomena other than disks could explain their mid-IR excesses. An unresolved close stellar companion cannot produce the observed IR-excess. For most of the stars in Table 1, their mid-IR excesses are only significant at [8.0]. A companion dwarf star of G, K, or M spectral class would raise the photometric flux at wavelengths ≤ 1 μm to a much greater degree than in the mid-IR, and such additional stellar components are inconsistent with the observed SEDs. Even with additional stellar companions, the [8.0] measurements are still above expected photospheric levels. If any of our targets are multiple star systems, the primary star dominates the SED and a diskless companion would not contribute significantly to the SED.

We investigated the GLIMPSE residual images after point-spread function fitting photometry and subtraction to rule out the possibility of systematic photometric errors. There were no significant residuals in the pixels at or surrounding each star's location. If larger photometric uncertainties in high background or highly structured background regions produced spurious signatures of $(K - 8)$ excesses, we would expect to see as many

TABLE 1
PHOTOMETRIC PARAMETERS FOR STARS WITH MID-IR EXCESSES

Reference ID	GLIMPSE ID	2MASS ID	K (mag)	$V-K$[a] (mag)	$J-K$[b] (mag)	$H-K$[c] (mag)	$K-[3.6]$[d] (mag)	$K-[4.5]$[e] (mag)	$K-[5.8]$[f] (mag)	$K-[8.0]$[g] (mag)	Spectral Type
1............	G284.3535−00.2021	10250358−5741409	11.89 (0.03)	−0.05 (0.17)	0.07 (0.04)	0.10 (0.04)	0.14 (0.04)	0.15 (0.05)	0.24 (0.07)	0.97 (0.14)	A3 V
2............	G284.1744−00.5141	10224039−5751461	12.47 (0.03)	−0.00 (0.43)	0.06 (0.04)	0.05 (0.04)	0.02 (0.04)	0.01 (0.05)	0.13 (0.15)	0.89 (0.12)	A2 V
3............	G283.8842−00.3361	10213378−5733229	11.97 (0.02)	−0.13 (0.17)	0.02 (0.03)	0.00 (0.03)	0.18 (0.03)	0.12 (0.04)	0.22 (0.07)	0.73 (0.09)	B9 V
4............	G284.1241−00.2429	10232673−5736249	10.92 (0.02)	0.86 (0.16)	0.11 (0.03)	0.03 (0.03)	0.14 (0.03)	0.14 (0.04)	0.22 (0.05)	0.53 (00.06)	A7 V
5............	G284.0185−00.1803	10230188−5729511	12.66 (0.03)	1.98 (0.44)	0.55 (0.04)	0.11 (0.04)	0.14 (0.04)	0.08 (0.05)	0.45 (0.11)	0.45 (0.08)	K0 V
6............	G284.0547−00.5695	10214145−5750415	12.73 (0.04)	0.99 (0.43)	0.21 (0.05)	0.07 (0.05)	0.10 (0.05)	0.11 (0.06)	0.40 (0.09)	1.27 (0.23)	B8 V
7............	G284.0719−00.1637	10232601−5730435	12.60 (0.03)	1.66 (0.43)	0.43 (0.04)	0.13 (0.04)	0.22 (0.04)	0.26 (0.05)	0.28 (0.09)	0.65 (0.08)	F3 IV
8............	G284.0110−00.1208	10231333−5726356	12.46 (0.04)	1.54 (0.43)	0.33 (0.05)	0.06 (0.05)	0.20 (0.05)	0.14 (0.05)	0.18 (0.09)	0.49 (0.07)	F5 IV
9............	G284.2320−00.1670	10242577−5736016	11.24 (0.02)	0.61 (0.43)	0.15 (0.03)	0.06 (0.03)	0.09 (0.03)	0.11 (0.03)	0.25 (0.05)	0.61 (0.04)	A5 V
10............	G284.0658−00.3254	10224485−5738431	11.51 (0.02)	1.35 (0.43)	0.34 (0.03)	0.07 (0.03)	0.11 (0.03)	0.08 (0.04)	0.22 (0.06)	0.55 (0.06)	G0 V
11............	G283.9773−00.3948	10215463−5739217	12.38 (0.02)	0.02 (0.23)	0.04 (0.03)	0.00 (0.04)	0.03 (0.04)	0.05 (0.05)	−0.01 (0.08)	0.37 (0.08)	B8 V
12............	G283.9935−00.1944	10224911−5729455	12.21 (0.02)	1.68 (0.43)	0.45 (0.03)	0.11 (0.03)	0.19 (0.04)	0.13 (0.05)	0.30 (0.07)	1.05 (0.06)	G5 V
13............	G283.9239−00.5103	10210640−5743271	12.09 (0.02)	0.97 (0.43)	0.27 (0.03)	0.03 (0.04)	0.12 (0.04)	0.14 (0.04)	0.22 (0.07)	0.70 (0.08)	F5 IV/V
14............	G283.9153−00.4337	10212181−5739183	12.80 (0.03)	1.34 (0.43)	0.30 (0.04)	0.07 (0.04)	0.05 (0.05)	0.07 (0.06)	0.41 (0.12)	0.94 (0.13)	F3 V
15............	G284.0478−00.1686	10231576−5730119	13.33 (0.05)	......	0.81 (0.06)	0.19 (0.06)	0.24 (0.06)	0.18 (0.08)	0.79 (0.19)	0.99 (0.15)	K5 V
16............	G283.9076−00.1997	10221550−5727151	10.90 (0.04)	......	0.95 (0.04)	0.22 (0.04)	0.18 (0.04)	0.14 (0.04)	0.22 (0.05)	0.51 (0.05)	G8 IV
17............	G283.9040−00.3687	10213333−5735398	12.06 (0.02)	......	0.83 (0.03)	0.17 (0.03)	0.18 (0.04)	0.14 (0.05)	0.41 (0.07)	0.58 (0.08)	K5 V
18............	G284.3417−00.2049	10245840−5741272	11.57 (0.04)	......	1.39 (0.06)	0.36 (0.06)	0.34 (0.05)	0.33 (0.05)	0.43 (0.07)	1.05 (0.12)	F8 Ve

NOTE.—Values in parentheses are 1 σ errors.
[a] Guide Star Catalog 2.2 V − 2MASS K.
[b] 2MASS J − 2MASS K.
[c] 2MASS H − 2MASS K.
[d] 2MASS K − IRAC [3.6], using zero points from (Cohen et al. 2003) in all colors.
[e] 2MASS K − IRAC [4.5].
[f] 2MASS K − IRAC [5.8].
[g] 2MASS K − IRAC [8.0].

TABLE 2
OTHER STARS WITH MID-IR EXCESSES

Reference ID	GLIMSPSE ID	2MASS ID	K^a (mag)	$V - K^b$ (mag)	$J - K^c$ (mag)	$H - K^d$ (mag)	$K - [3.6]^e$ (mag)	$K - [4.5]^f$ (mag)	$K - [5.8]^g$ (mag)	$K - [8.0]^h$ (mag)	Spectral Type	$E(K - 8)$ (mag)
19....................	G283.9403−00.2636	10221243−5731324	9.81 (0.02)	0.52 (0.05)	0.07 (0.03)	0.06 (0.03)	0.51 (0.03)	0.71 (0.03)	0.92 (0.03)	1.32 (0.02)	B2 V (weak Be)	1.43
20....................	G284.1728−00.2039	10235451−5736004	10.63 (0.02)	0.49 (0.06)	0.08 (0.03)	0.00 (0.03)	0.54 (0.03)	0.61 (0.03)	0.73 (0.05)	1.03 (0.09)	B1 V (weak Be)	1.08
21....................	G284.1277−00.5835	10220574−5753460	10.60 (0.02)	3.91 (0.44)	0.77 (0.03)	0.28 (0.03)	0.27 (0.03)	0.41 (0.03)	0.49 (0.04)	1.48 (0.06)	B5 Vneb	1.23
22....................	G284.0335−00.2091	10230066−5731474	12.74 (0.03)	1.68 (0.44)	0.39 (0.04)	0.11 (0.04)	0.15 (0.04)	0.22 (0.05)	0.29 (0.12)	0.60 (0.12)	F5 II	0.57
23....................	G284.2642−00.3156	10240243−5744359	8.65 (0.03)	. . .	0.84 (0.04)	0.16 (0.05)	0.40 (0.05)	0.75 (0.05)	1.50 (0.03)	3.84 (0.03)	O4 V((f))	4.08
24....................	G284.0501−00.2464	10225795−5734130	11.50 (0.02)	. . .	0.98 (0.03)	0.23 (0.03)	0.23 (0.03)	0.19 (0.03)	0.29 (0.06)	0.75 (0.06)	G8 II	0.70
25....................	G283.9567+00.1258	10235162−5712213	13.04 (0.03)	. . .	0.38 (0.04)	0.08 (0.04)	0.18 (0.05)	0.11 (0.06)	0.43 (0.17)	0.59 (0.09)	G8 III	0.54
26....................	G283.9776+00.1738	10241078−5710353	13.03 (0.02)	. . .	0.39 (0.03)	0.07 (0.03)	0.09 (0.04)	0.10 (0.06)	0.45 (0.24)	0.63 (0.13)	F5 II	0.61
27....................	G284.2980−00.5951	10230784−5759512	7.49 (0.02)	1.44 (0.03)	0.58 (0.04)	0.38 (0.06)	0.44 (0.03)	0.70 (0.03)	0.90 (0.03)	1.24 (0.02)	B	1.15
28....................	G283.9831−00.5360	10212249−5746404	13.39 (0.04)	1.80 (0.44)	0.54 (0.05)	0.21 (0.06)	0.15 (0.05)	0.12 (0.08)	. . . (. . .)	1.62 (0.20)	G2 V	1.60
29....................	G284.0107−00.1372	10230932−5727250	14.05 (0.05)	2.08 (0.45)	0.48 (0.05)	0.11 (0.05)	0.11 (0.07)	0.06 (0.09)	. . . (. . .)	1.58 (0.20)	F8 V	1.53
30....................	G283.9764−00.1365	10225656−5726168	13.36 (0.04)	0.63 (0.02)	0.63 (0.05)	0.23 (0.05)	0.30 (0.06)	0.36 (0.07)	. . . (. . .)	1.09 (0.14)	A7 V	1.11
31....................	G284.4730−00.2456	10253880−5747417	12.33 (0.03)	0.65 (0.43)	0.18 (0.04)	0.03 (0.04)	0.06 (0.04)	0.09 (0.05)	0.23 (0.11)	0.34 (0.07)	A7 V	0.36
32....................	G283.9309−00.0712	10225509−5721302	12.58 (0.03)	1.91 (0.44)	0.53 (0.04)	0.11 (0.17)	0.04 (0.04)	0.01 (0.05)	0.24 (0.10)	0.44 (0.11)	G0 V	0.40
33....................	G283.9809−00.1931	10224464−5730119	12.78 (0.02)	. . .	0.43 (0.04)	0.11 (0.04)	0.12 (0.04)	0.05 (0.05)	0.12 (0.17)	0.52 (0.21)	F8 V	0.52

NOTE.—Values in parentheses are 1 σ errors.
[a] 2MASS K magnitude.
[b] Guide Star Catalog 2.2 $V -$ 2MASS K.
[c] 2MASS $J -$ 2MASS K.
[d] 2MASS $H -$ 2MASS K.
[e] 2MASS $K -$ IRAC [3.6].
[f] 2MASS $K -$ IRAC [4.5].
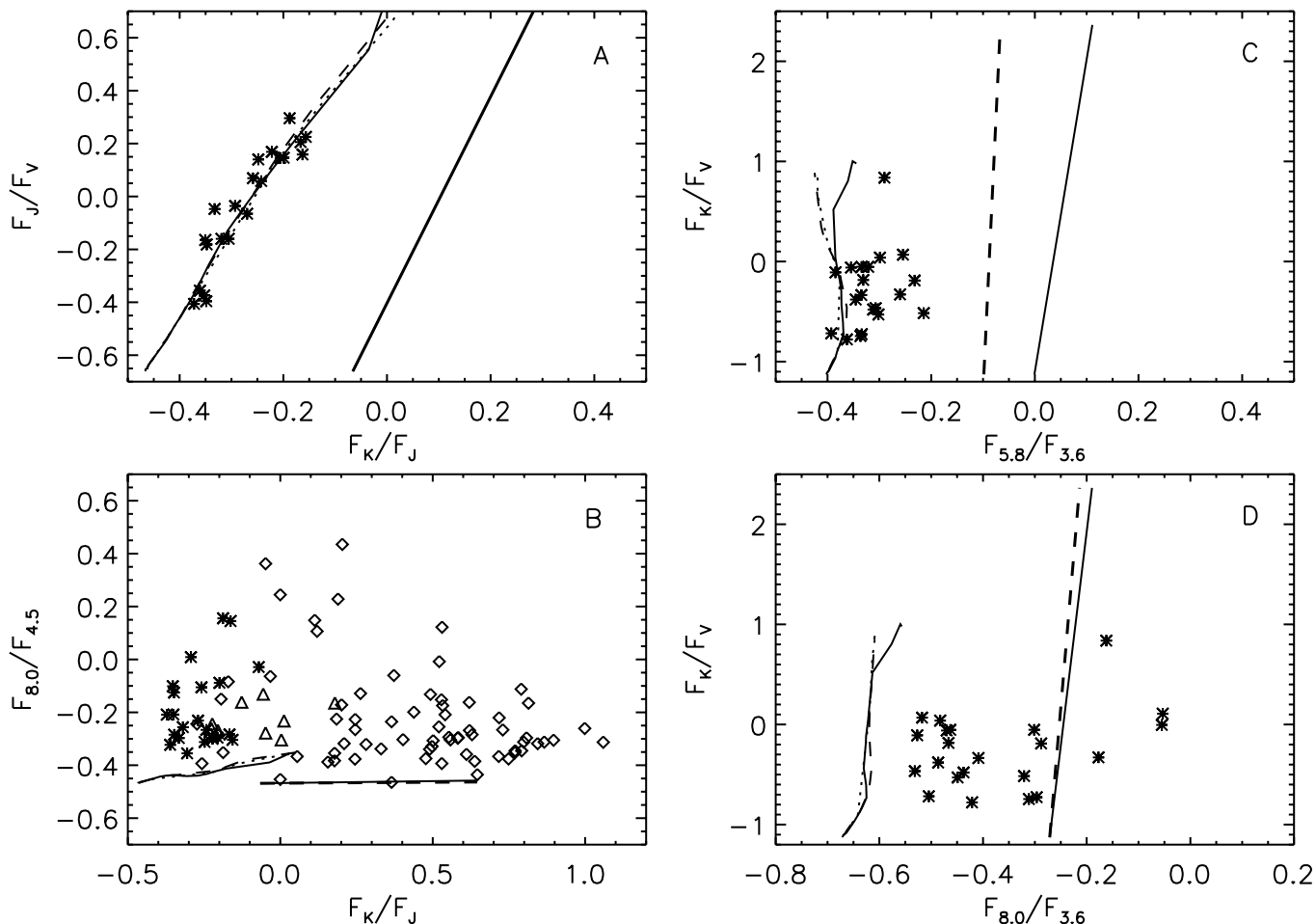[g] 2MASS $K -$ IRAC [5.8].
[h] 2MASS $K -$ IRAC [8.0].

Fig. 3.—Color-color plots of stars in the GLIMPSE OSV region. The large black asterisks mark classified stars with a $(K-8)$ excess. The triangles mark classified stars with a $(K-8)$ excess that did not have a V-band GSC measurement. The diamonds denote spectroscopic target stars that were too faint or featureless for spectral classification. Most of the diamonds are consistent with being heavily reddened stars. The black vectors are the extinction vector of Li & Draine (2001). The dashed vectors are the extinction law of Indebetouw et al. (2005) in the mid-IR. Both sets of extinction vectors represent $A_V = 10$ and are offset from the stellar sequence for clarity. The solid thin line is for the theoretical main sequence, the dash-dotted line is for the giant sequence, and the dashed line is for the supergiant sequence. (De Jager & Nieuwenhuijzen 1987; Schmidt-Kaler 1982; Johnson, 1966).

stars with negative $E(K-8)$ as positive $E(K-8)$. The distribution in Figure 2, however, shows only significant positive $E(K-8)$ values. If the excess is due to only polycyclic aromatic hydrocarbon (PAH) features, we would expect to see an enhancement at [3.6], [5.8], and [8.0] with respect to [4.5] since [4.5] is devoid of PAH features. None of our excess sources exhibit this enhancement.

Thermal bremsstrahlung emission could possibly explain the $E(K-8)$ values seen in the three early B stars and one O star listed in Table 2. These stars generally have all four IRAC measurements in excess of the photospheric model values. An optically thin, thermal bremsstrahlung component was included in the modeling of their SEDs. The luminosity of the bremsstrahlung component was allowed to vary as a free parameter along with extinction and distance. These models with bremsstrahlung components fit the SEDs much better than the models with a single blackbody component. A blackbody component model with a single temperature is insufficient to fit all four measurements in excess of the photosphere. Since these are ionizing stars and they fit a thermal bremsstrahlung model, we feel that this is the most likely explanation for the mid-IR excess of these four stars.

In conclusion, we note that the characteristic temperature of the blackbody component that creates a significant excess at 8 μm, but not at shorter wavelengths, is ~400 K with a peak at

~7 μm. Even the coolest known brown dwarfs (Burgasser et al. 2000; Burrows et al. 2001) have temperatures of ~700–750 K, and Jupiter-like planets would be insufficiently luminous to create the observed infrared excesses. We conclude that the source of the mid-IR excess for the stars in Table 1 is probably warm ~400 K dust.

4. DISCUSSION

An SED of β Pictoris, the prototype debris disk system, is shown in Figure 4 for comparison to the excess candidates. Figure 4 also shows the appropriate Kurucz model. The SED comprises L (3.45 μm), M (4.80 μm), N (10.1 μm), and Q (20 μm) measurements from Backman et al. (1992). The Q-band measurement was included so that the number of data points and the wavelength range was similar for both β Pictoris's model and the G18 stars (eight measurements and four free parameters in the model). The GSC and 2MASS measurements were used to model β Pictoris in a manner equivalent to that for the G18 stars. Comparing the 2MASS photometry to near-IR measurements in the literature for β Pictoris shows that the near-IR photometry is consistent, but 2MASS data have much larger uncertainties of approximately 20%. Our spectrophotometric distance of 22.5 $\pm$ 3.0 pc for β Pictoris is consistent with the *Hipparcos* distance of 19.28 $\pm$ 0.19 pc.
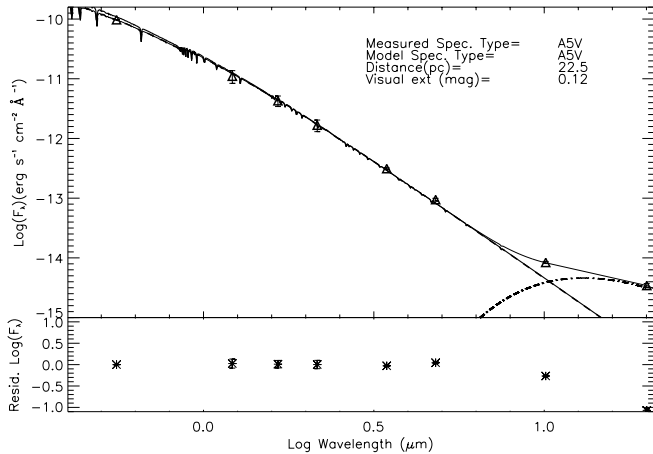
Fig. 4.—SED of β Pictoris using GSC, 2MASS, and Backman et al. (1992) measurements. Like most of our candidate sources, β Pictoris shows an excess at longer mid-IR wavelengths. β Pictoris did show a small excess at 4.80 μm in Backman et al. (1992). The thick solid line is the Kurucz model ($T_{\mathrm{eff}} = 8200\,\mathrm{K}$, $\log g = +4.29$), the thick dashed line is the Kurucz model with extinction applied, the dot-dashed line is the SED of the blackbody component with $T = 223\,\mathrm{K}$, and the thin line is the combination of the Kurucz model with extinction plus the SED of the disk component. The residual plots below are shown before the addition of the blackbody component. They demonstrate that at longer wavelengths β Pictoris deviates from the model photosphere.

In order to estimate the sizes and temperatures of any dust disks for the G18 stars, we modeled the excess in each star as a single blackbody with temperature and fractional bolometric disk-to-star luminosity ratio, L_{IR}/L_*, as free parameters. This assumption, although simplistic, yields a rough approximation to the temperatures and L_{IR}/L_* of the dust disks, given the limited number of photometric points available. We searched a grid of blackbody temperatures and fractional disk luminosities to find best fits to the observed data. The temperature grid ranged from 100 to 1100 K in steps of 1 K. This model was used to estimate the most probable parameters for the dust disks. For our model of β Pictoris, we found a single temperature for the excess to be 223^{+4}_{-4} K with the disk emitting $0.0019^{+0.0002}_{-0.0002}$ the luminosity of the star. In comparison, Gillett (1986) fit a single-temperature blackbody to both mid-IR *and* far-IR data, from which they infer a temperature of 103 K and a fractional luminosity of 0.003 for β Pictoris. By fitting the mid-IR data alone we may be overestimating the disk temperature or just measuring the hotter inner portion of a larger disk. Chen & Jura (2001) found the color temperature of ζ Leporis to be 370 K, but they note that if they only fit the data at wavelengths greater than 10 μm the disk temperature is better fit by a 230 K blackbody. Backman et al. (1992) use a two-disk component for β Pictoris and find the inner disk temperatures to range from 200–400+ K depending on the model used. Therefore the temperature we estimate for the debris disk is consistent with the range of disk temperatures given in Backman et al. (1992) from a variety of more sophisticated models.

We investigated the likelihood of other disk temperature/fractional luminosity combinations using a Monte Carlo simulation to determine the uncertainties on our derived disk and star parameters. The Monte Carlo code adds Gaussian noise to each of the photometric data points (based on their 1 σ photometric errors) and then recomputes the most probable distance, visual extinction, blackbody temperature, and fractional blackbody luminosity. Figure 5 shows a plot of the Monte Carlo simulation results for β Pictoris. The photometry and model constrain the temperature and fractional luminosity to a small
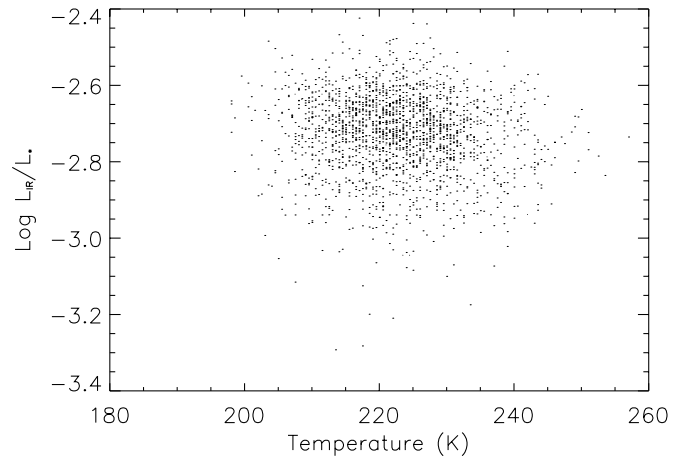

Fig. 5.—Plot of the Monte Carlo simulation for β Pictoris. The simulation demonstrates that temperature and fractional luminosity are well constrained to 223^{+4}_{-4} and fractional luminosity $0.0019^{+0.0002}_{-0.0002}$.

region of the parameter space. Even a few near and mid-IR photometric measurements effectively constrain the temperatures and fractional disk luminosities. Figure 6 shows the distribution functions of distance (before adding the 15% stellar radii uncertainty), visual extinction, blackbody temperature, and fractional luminosity for β Pictoris. Both the blackbody temperature and fractional luminosity are well constrained in this simulation. Spectrophotometric uncertainties are primarily due to the assumption for the stellar radii uncertainties but are still well constrained. With only the visual measurement, there is some variation in extinction but extinction is typically low. Distributions for all the derived parameters are nearly Gaussian.

We then conducted the same analysis on our candidate stars. In a small fraction of the Monte Carlo simulations, ≤5% for most stars, the best-fit parameters require a fractional disk-to-star luminosity ratio greater than unity. We discard these Monte Carlo iterations as unphysical. In order for the luminosity of the disk to exceed the luminosity of the star, the star would have to be embedded in a region that required reemission of absorbed stellar light, or generation of energy by the disk. This would occur in early protostars, Class 0 or I, but not in more evolved pre–main-sequence stars. Three stars, G284.1744−00.5141, G284.0110−00.1208, and G283.9773−00.3948, had greater than 10% of their Monte Carlo simulations yield unphysical fractional disk luminosities. These three stars have an excess only at 8 μm, which provides weaker constraints on the fractional disk luminosity and temperature. Table 3 lists derived parameters and their uncertainties on the basis of the median values of the Monte Carlo simulation.

Figure 7 shows the SED for one of our G18 stars, the A3 V star G284.3535−00.2021. The thick solid line is the Kurucz model, the dot-dashed line is the SED of the disk component, and the thin line is the combination of the Kurucz model with extinction plus the SED of the disk component.

Figure 8 shows the results for 2000 Monte Carlo iterations, demonstrating that higher temperatures paired with lower fractional luminosities occur more readily than lower temperatures with higher fractional luminosities. This plot of fractional disk luminosity versus temperature demonstrates that there is an anti-correlation between fractional disk luminosity and temperature. When blackbody temperature is high, the fractional disk luminosity is low, and when temperature is low, fractional disk luminosity is high. The median temperature from the simulations is 385 K (i.e., ∼160 K warmer than β Pictoris), consistent with

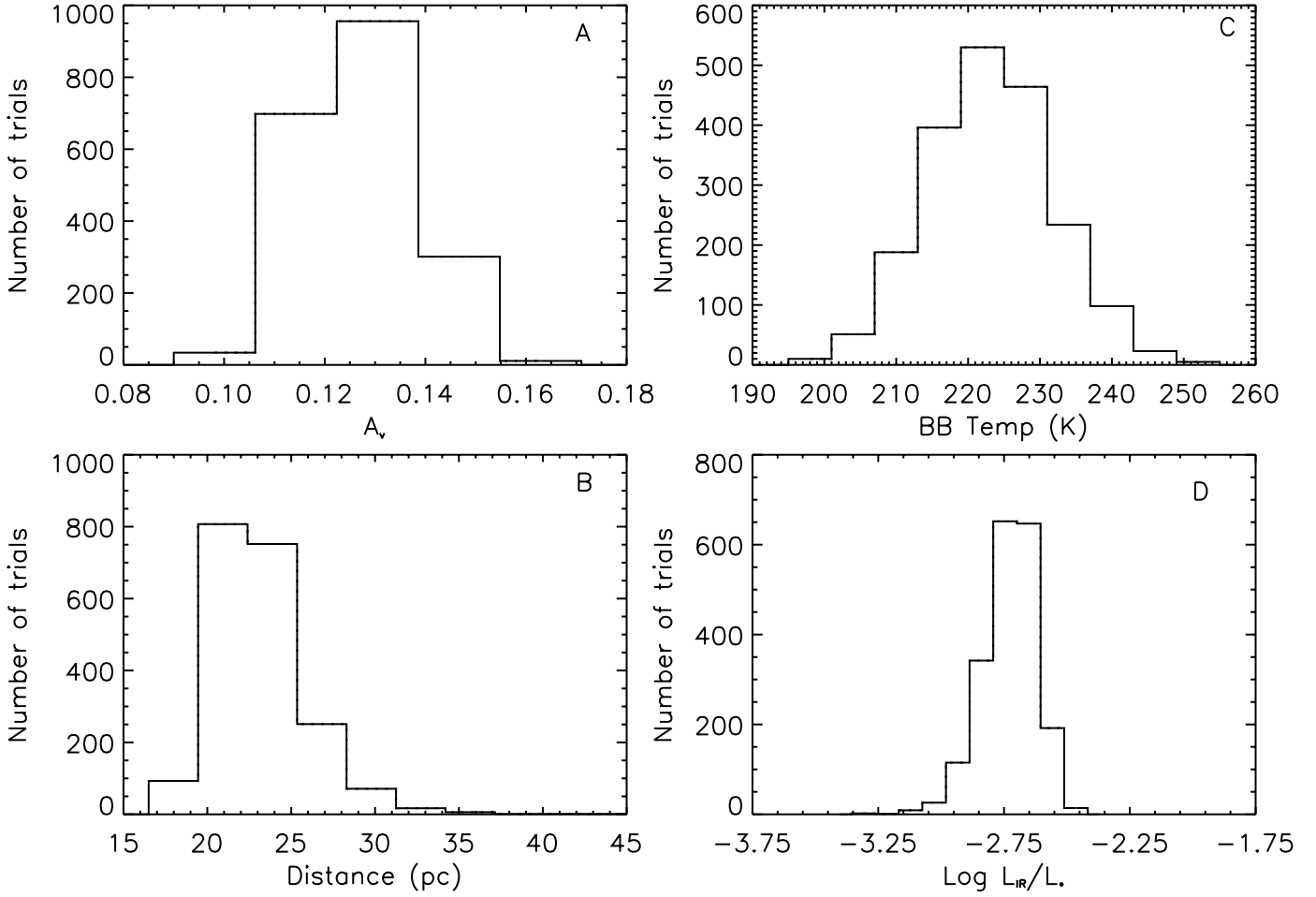Fig. 6.—Histograms of (*a*) derived extinction, (*b*) spectrophotometric distance, (*c*) blackbody temperature, and (*d*) fractional luminosity for β Pictoris using a Monte Carlo simulation.

TABLE 3
DERIVED PARAMETERS FOR CANDIDATE β PICTORIS ANALOGS

Reference ID	GLIMPSE ID	2MASS ID	Spectral Type	$E(K\text{-}8)$ (mag)	Distance[a] (pc)	A_v (mag)	Temperature[b] (K)	L_{IR}/L_*[c]	T_{eff}[d] (K)	$\log g$[e] (11)
1	G284.3535−00.2021	10250358−5741409	A3 V	1.00	1068^{+160}_{-160}	$0.00^{+0.07}_{-0.00}$	385^{+70}_{-56}	$0.0043^{+0.0014}_{-0.0010}$	8200	+4.29
2	G284.1744−00.5141	10224039−5751461	A2 V	0.92	1398^{+210}_{-210}	$0.00^{+0.08}_{-0.00}$	300^{+37}_{-30}	$0.0059^{+0.0025}_{-0.0014}$	8200	+4.29
3	G283.8842−00.3361	10213378−5733229	B9 V	0.77	1938^{+290}_{-290}	$0.00^{+0.08}_{-0.00}$	482^{+113}_{-95}	$0.0018^{+0.0004}_{-0.0002}$	9520	+4.14
4	G284.1241−00.2429	10232673−5736249	A7 V	0.54	563^{+85}_{-85}	$0.23^{+0.09}_{-0.08}$	620^{+129}_{-129}	$0.0033^{+0.0005}_{-0.0004}$	7200	+4.34
5	G284.0185−00.1803	10230188−5729511	K0 V	0.43	593^{+90}_{-90}	$0.17^{+0.19}_{-0.17}$	801^{+74}_{-56}	$0.0078^{+0.0012}_{-0.0010}$	5250	+4.49
6	G284.0547−00.5695	10214145−5750415	B8 V	1.24	3073^{+475}_{-460}	$1.47^{+0.19}_{-0.16}$	350^{+42}_{-46}	$0.0137^{+0.0076}_{-0.0030}$	11900	+4.04
7	G284.0719−00.1637	10232641−5730435	F3 IV	0.62	963^{+145}_{-150}	$0.78^{+0.32}_{-0.20}$	803^{+95}_{-149}	$0.0081^{+0.0011}_{-0.0009}$	6440	+4.34
8	G284.0110−00.1208	10231333−5726356	F5 IV	0.46	918^{+140}_{-140}	$0.62^{+0.25}_{-0.23}$	838^{+181}_{-240}	$0.0057^{+0.0009}_{-0.0009}$	6440	+4.34
9	G284.2320−00.1670	10242577−5736016	A5 V	0.61	773^{+115}_{-115}	$0.41^{+0.21}_{-0.21}$	508^{+110}_{-73}	$0.0030^{+0.0005}_{-0.0005}$	8200	+4.29
10	G284.0658−00.3254	10224485−5738431	G0 V	0.55	493^{+75}_{-75}	$0.04^{+0.23}_{-0.04}$	567^{+106}_{-85}	$0.0051^{+0.0007}_{-0.0009}$	6030	+4.49
11	G283.9773−00.3948	10215463−5739217	B8 V	0.42	2798^{+420}_{-420}	$0.41^{+0.17}_{-0.17}$	460^{+282}_{-102}	$0.0009^{+0.0002}_{-0.0002}$	11900	+4.04
12	G283.9935−00.1944	10224911−5729455	G5 V	1.03	553^{+85}_{-85}	$0.27^{+0.29}_{-0.09}$	424^{+50}_{-44}	$0.0154^{+0.0025}_{-0.0025}$	5770	+4.49
13	G283.9239−00.5103	10210640−5743271	F5 IV/V	0.71	793^{+120}_{-120}	$0.00^{+0.29}_{-0.00}$	542^{+103}_{-81}	$0.0050^{+0.0009}_{-0.0005}$	6440	+4.34
14	G283.9153−00.4337	10212181−5739183	F3 V	0.93	1068^{+165}_{-175}	$0.39^{+0.13}_{-0.24}$	395^{+54}_{-34}	$0.0115^{+0.0027}_{-0.0017}$	6440	+4.34
15	G284.0478−00.1686	10231576−5730119	K5 V	0.91	608^{+95}_{-90}	...	654^{+60}_{-54}	$0.0309^{+0.0022}_{-0.0026}$	4350	+4.54
16	G283.9076−00.1997	10221550−5727151	G8 IV	0.49	268^{+40}_{-40}	...	723^{+52}_{-67}	$0.0066^{+0.0010}_{-0.0007}$	5250	+4.49
17	G283.9040−00.3687	10213333−5735398	K5 V	0.50	338^{+50}_{-50}	...	776^{+33}_{-74}	$0.0148^{+0.0029}_{-0.0073}$	4350	+4.54
18	G284.3417−00.2049	10245840−5741272	F8 Ve	1.05	513^{+75}_{-75}	...	560^{+84}_{-43}	$0.0108^{+0.0002}_{-0.0002}$	6030	+4.49

[a] Spectrophotometric distance.
[b] Best-fit blackbody model temperature for excess.
[c] Best-fit disk-to-star luminosity ratio.
[d] Effective temperature for the adopted Kurucz model.
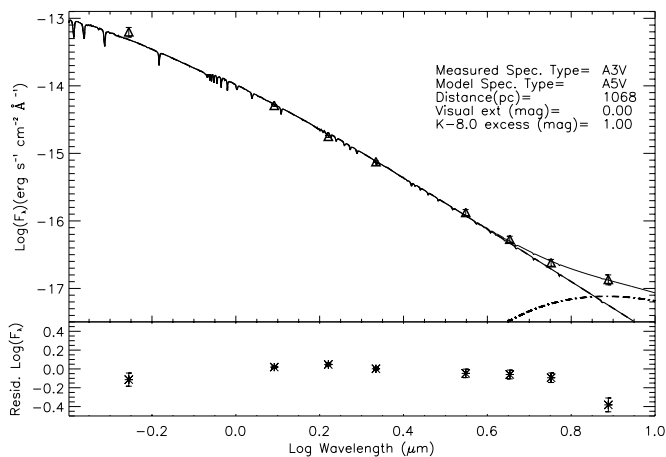[e] Value of $\log g$ for the adopted Kurucz model.

Fig. 7.—SED of G284.3535−00.2021, one of our candidate β Pictoris analogs. The thick solid line is the Kurucz model, the dot-dashed line is the SED of the disk component, and the thin line is the combination of the Kurucz model with extinction plus the SED of the disk component. The residual plots below are shown before the addition of the blackbody component. G284.3535−00.2021 shows a significant deviation from the photosphere at 8 μm.
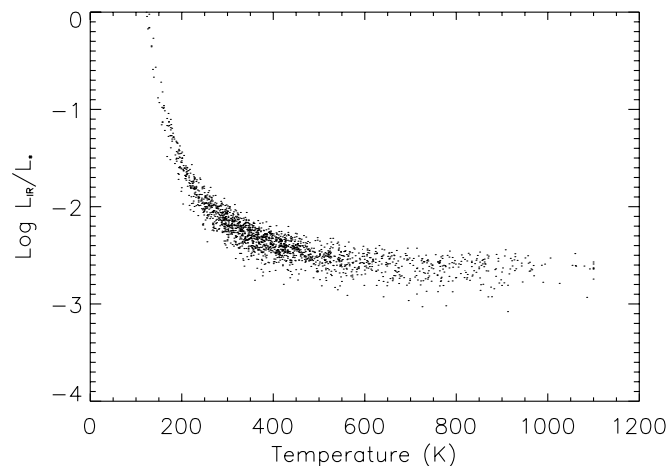

Fig. 8.—Scatter plot of the best-fit blackbody temperature vs. fractional disk-to-star luminosity ratio based on 2000 Monte Carlo simulations for G284.3535−00.2021. A wide range of temperatures and fractional luminosities are allowed for the given photometric measurements, but these allowed values are constrained to a narrow region of parameter space. The majority of the simulations indicate preferred disk temperatures of 315–440 K and fractional disk-to-star luminosities of 0.0033–0.0057, as shown in the histograms in Fig. 9.

the observation that the excess appears at shorter wavelengths in G284.3535−00.2021. The models constrain the temperature to 385^{+70}_{-56} K and the fractional disk luminosity to $0.0043^{+0.0014}_{-0.0010}$.

Figure 9 shows the distribution of distance (before adding the 15% stellar radii uncertainty), visual extinction, temperature, and fractional luminosity for G284.3535−00.2021 determined from Monte Carlo simulations. This distribution is much broader than that for β Pictoris due to our limited ability to constrain maximum possible temperatures with data shortward of 8 μm. Longer wavelength data, in both the mid- and far-IR, would allow us to better constrain the temperature and fractional luminosity. The majority of the simulations for this star produced minimal values for visual extinction, which is reflected in the histogram. This is due to the optical measurement and the large uncertainty associated with it.

Table 3 lists the derived parameters and their uncertainties for all 18 main-sequence, non O and B stars with an excess (in the G18 sample). The temperatures for the excesses range from 220 to 820 K, with fractional luminosities ranging from 10^{-3} to 10^{-2}. Figure 10 shows both temperature and fractional luminosity ratio histograms for the remaining 17 stars in the G18 sample. For star 11 a large portion of the fractional luminosity ratio is below 10^{-3} and is therefore off the scale. This is because there is a significant excess at only [8.0]. G284.0110−00.1208 and G284.0719−00.1637 have broad distributions, again due to the weaker constraints on the excess. Figure 10 demonstrates the large variation in temperature and fractional luminosity distribution between stars. Figure 11 shows the distribution of both temperature and fractional luminosity for all G18 stars. The median temperature for the sample is ∼500 K. There does not appear to be a correlation between either temperature or fractional disk luminosity with spectral type, but the sample is small. Future work may reveal a correlation of either disk temperature or fractional luminosity with spectral type.

4.1. Protostellar Disk or Debris Disk?

Lagrange et al. (2000) suggest a definition of debris disks using four criteria. These criteria include the bolometric fractional disk-to-star luminosity $\leq 10^{-3}$, the mass of the gas and dust to be below $10^{-2}\,M_{\odot}$, the dust mass significantly greater than the gas mass, and the grain destruction time much less than the stel-

lar age. Our limited data only allow comparisons based on the fractional bolometric luminosity.

Since $L_{\mathrm{IR}}/L_* \leq 0.1$ for all of the G18 stars, these stars are not primordial and may be in a transitional phase from protostellar to debris disk or debris disks themselves. Although these stars have blue spectra that lack emission lines, except G284.3417−00.2049 ,which exhibits Hβ emission and appear to be main-sequence, we cannot rule out Hα emission. Weak Hα emission, without Hβ emission, could imply that the star is pre−main-sequence. We cannot rule out the possibility that the stars may have primordial disks, but the disks are most likely to be debris disks. Protostars typically have $L_{\mathrm{IR}}/L_* \geq 0.1$ and debris disks typically have $L_{\mathrm{IR}}/L_* \sim 10^{-3}$ (Lagrange et al. 2000; Backman & Paresce 1993). Since G284.1744−00.5141, G284.0110−00.1208, and G283.9773−00.3948 had a large number of their Monte Carlo iterations discarded because they were unphysical, their fractional disk luminosities may be greater than tabulated in Table 3. These stars may be protostellar in nature since the models allow higher fractional luminosities, but their derived luminosities, omitting the unphysical simulations, are still consistent with debris disks. Mid-IR spectral analysis of the stars in Table 3 would reveal whether the 10 μm silicate feature is present and would be a useful tool in the characterization of mid-IR excesses around main-sequence stars. The absorption (embedded protostar), emission (pre−main-sequence), or lack of the 10 μm silicate feature (debris disk) is loosely related to the evolutionary progression of a circumstellar disk (Kessler-Silacci et al. 2005). However, the debris disks studied by Kessler-Silacci et al. (2005) contained debris disks that only exhibited far-IR excesses. β Pictoris, a mid-IR debris disk system, does have a 10 μm silicate emission feature. A useful comparison would be to determine whether this sample of mid-IR debris disk systems also exhibits a 10 μm silicate emission feature.

5. G284.2642−00.3156

One especially interesting star that exhibited a mid-IR excess is G284.2642−00.3156. The optical spectrum of this early-type star is shown in Figure 12. Using the OB star spectral atlas of Walborn & Fitzpatrick (1990), we classify this star as O4 V((f)). The classification is based on the relative strength of He I, He II,
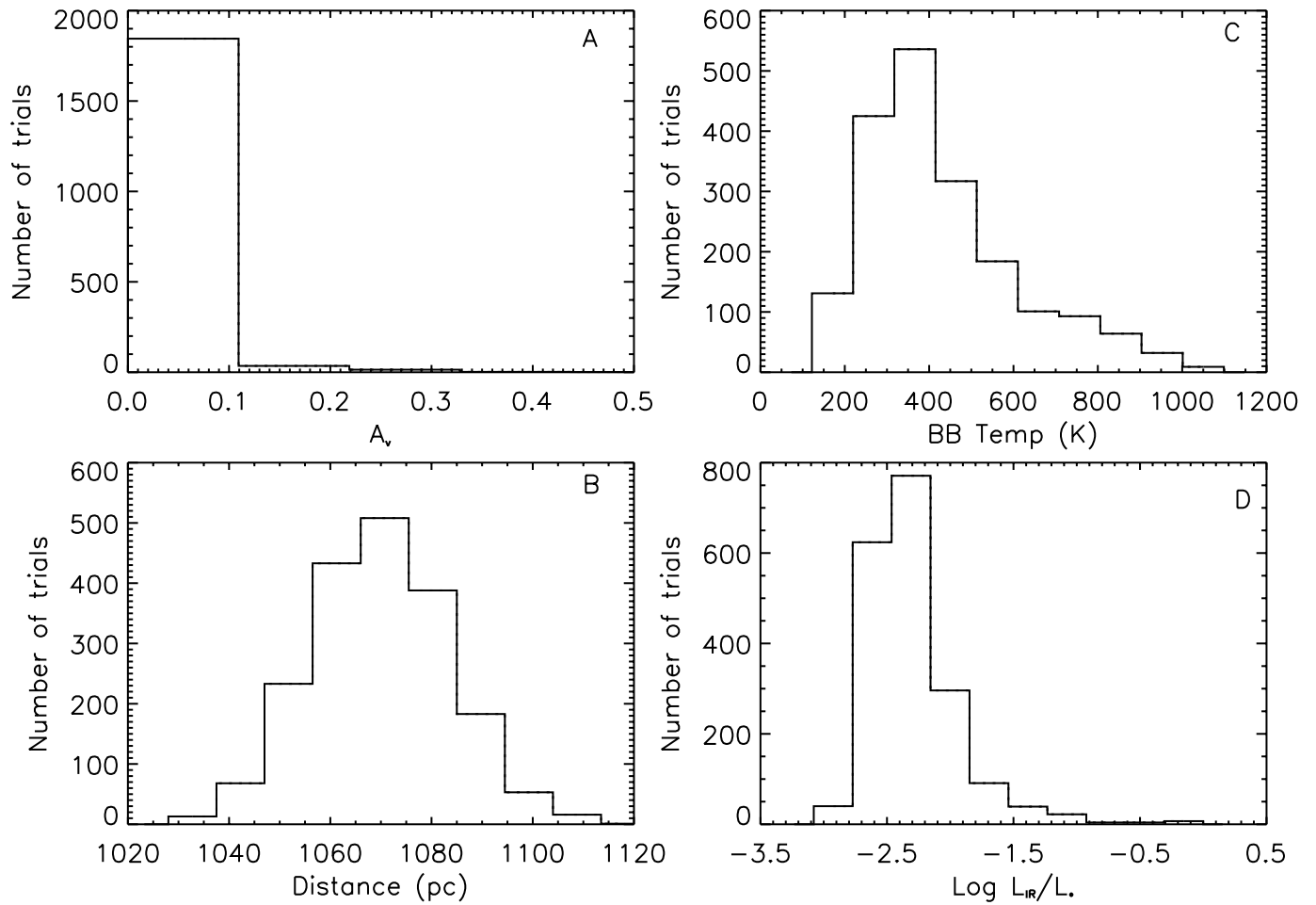
Fig. 9.—Histograms of (*a*) derived extinction, (*b*) spectrophotometric distance, (*c*) blackbody temperature, and (*d*) fractional luminosity for G284.3535−00.2021. The distributions for the derived parameters constrain the possible values, but the dispersion is larger than in the simulations of β Pictoris because the models are not as tightly constrained without data longward of 8 μm.
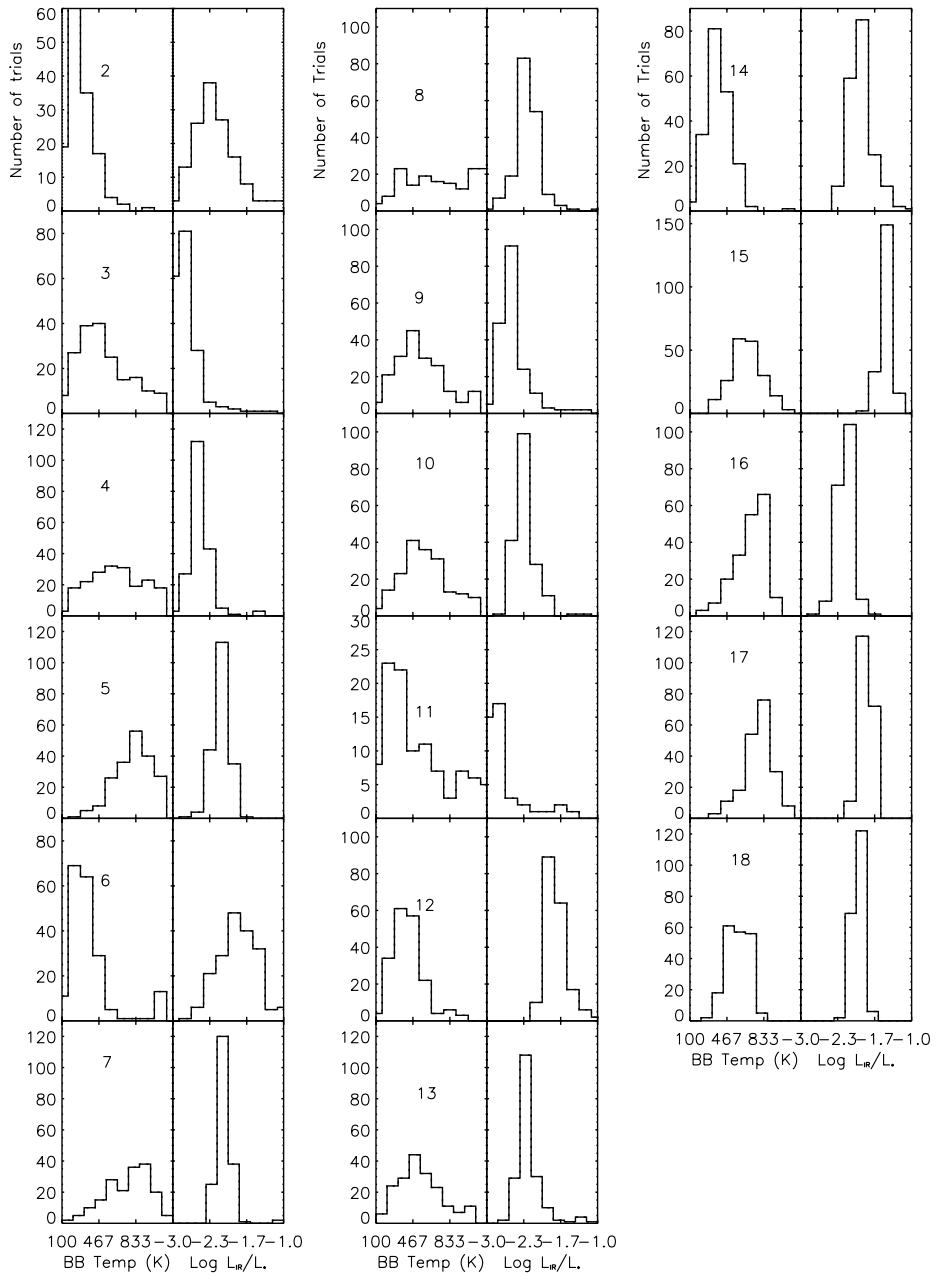
FIG. 10.—Histograms of both temperature and fractional luminosity for the remaining 17 stars in Table 3. The reference number in the figure refers to the star identification in this paper.
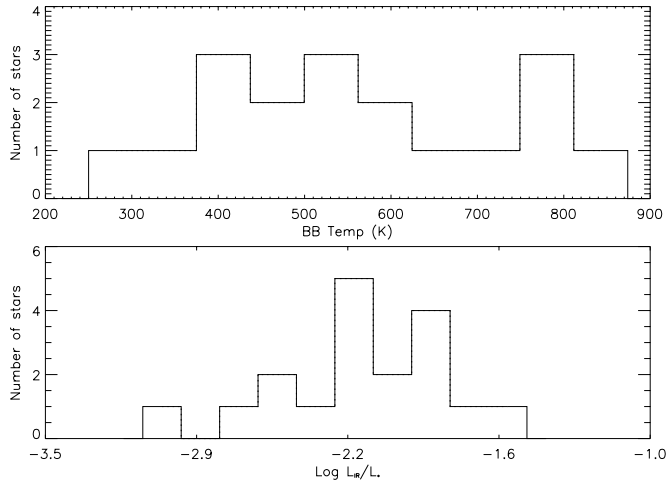
FIG. 11.—Histograms of both temperature and fractional luminosity for the median values derived for the G18 stars in Table 3. Although all the stars exhibit a mid-IR excess, there is a broad range of both temperatures and fractional luminosities for sample.

FIG. 13.—[3.6] *Spitzer* IRAC image showing both Westerlund 2 and the O4 V((f)) star. The position of the O star is shown by a white box. Diffuse emission in this band is attributed to known PAH features.

and the hydrogen Balmer series. Figure 12 shows that for this star, weak N III 4634–4640–4642 Å appears in emission and a strong He II 4686 Å appears in absorption implies that the star is earlier than O5. He I is present in absorption but is very weak. This implies that the star is later than O3, since an O3 lacks He I absorption. We did not see any N IV 4058 Å emission or any significant N V 4604 or 4620 Å absorption. He II 4686 Å is seen in absorption. These imply that the star is not a supergiant or giant.

Figures 13 and 14 show GLIMPSE [3.6] and [8.0] images in the region surrounding G284.2642−00.3156, including Westerlund 2. G284.2642−00.3156 is marked by the white box. The [3.6] image shows that G284.2642−00.3156 is surrounded by a grouping of faint stars that are partially blended with the O4 star at the 1″22 angular resolution of the IRAC 3.6 μm array. We determine a spectrophotometric distance to this star of 3233^{+540}_{-535} pc with a visual extinction of $5.63^{+0.01}_{-0.30}$. The [8.0] image shows a nearly circular ring with radius of $\sim38''$ surrounding the O star. At a distance of 3.5 kpc, the ring around the star would be 0.65 pc in diameter. This could be a windblown
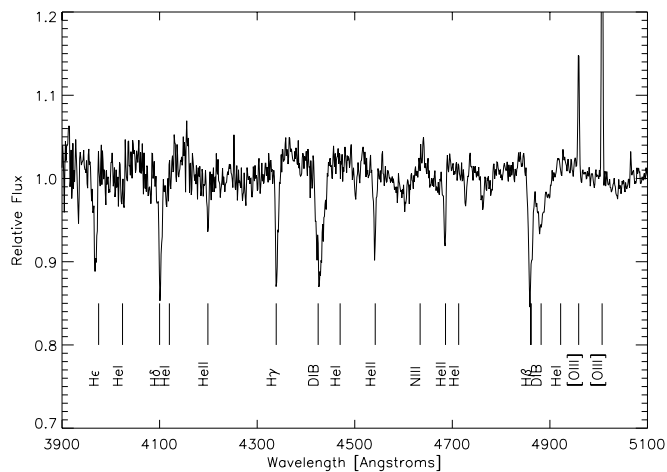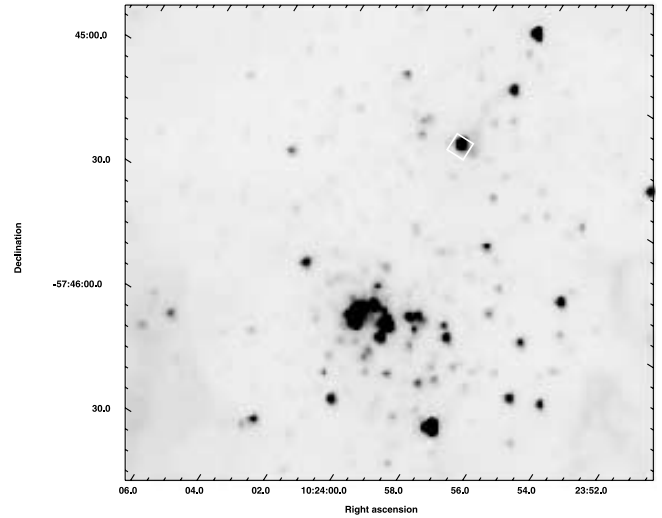
shell illuminated by the star. There is also an irregular linear feature extending 29″ from the star in the northwest direction. This feature may be a nearby cloud illuminated by the star, or it may trace the relative motion of the star through the interstellar medium surrounding Westerlund 2.

Using the images of Moffat et al. (1991), we identify G284.2642−00.3156 as their star 18, which they find to be the most luminous star in the cluster. They type this star as an O7 V, but they note that its absolute luminosity is brighter than that of an O7 V. Moffat et al. conclude that since the star appears isolated, it must, by color and luminosity arguments, be a supergiant if it lies at the distance of the cluster. Our new classification results in an earlier spectral type with an extinction that is still consistent with cluster membership but a distance that is not consistent with the 7.9 kpc by Moffat et al. (1991). We note that the distance we find for the O4 V((f)) star is inconsistent

FIG. 12.—Optical spectrum of G284.2642−00.3156 with stellar hydrogen and helium lines marked. The lack of strong He I absorption lines but strong He II lines make this a very early O star, probably an O4. The diffuse interstellar band feature at 4430 and 4882 Å is consistent with the high extinction ($A_V = 5.6$) to this star (Herbig 1995). The [O III] emission lines reveal the presence of ionized gas near the star.
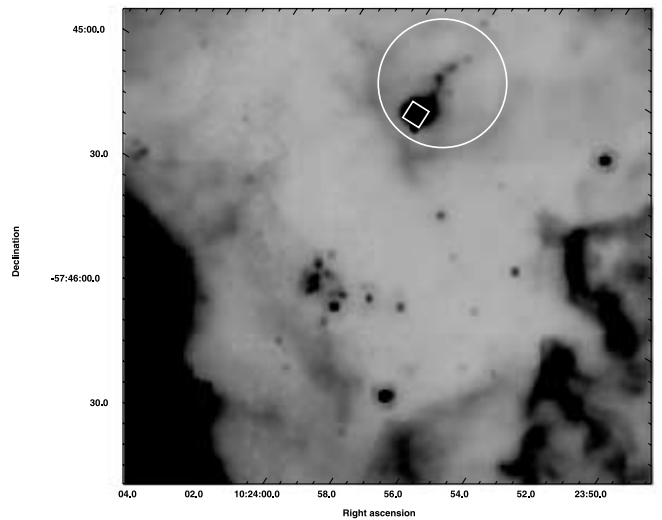

FIG. 14.—[8.0] *Spitzer* IRAC image showing both Westerlund 2 and the O4 V((f)) star. The position of the O star is shown by a white box. The [8.0] image shows a circular emission ring around the star, although the star is not centered within this ring. The ring and the irregular linear feature extending to the northwest from the star may trace molecular material or dust illuminated by the star. The diffuse emission is attributed to known PAH features in the [8.0] band.

with the Carraro & Munari (2004) cluster distance of 6.3 kpc but still consistent with the wide variation of distances found for this cluster (Churchwell et al. 2004). If this star is a cluster member, it would be the earliest known member. Moffat et al. (1991) assumed a cluster age of 2–3 Myr based on the presence of the O7 stars. The proximity of WR 20b to the cluster may imply an older age of 3–5 Myr if it is also a cluster member (Shara et al. 1991). The lifetime for an O4 is on the order of 3 Myr (for a 60 $M_{\odot}$ star with $Z = 0.02$; Meynet et al. 1994). G284.2642−00.3156 lies 1′ from the cluster center, which corresponds to a minimum projected separation of 1 pc if the star is at a distance of 3.5 kpc. In order to travel 1 pc in 3 Myr or less, a modest space velocity of ≥ 0.3 km s^{-1} is required. Thus the reddening and projected separation of the O4 star are consistent with cluster membership and origin. This implies that Westerlund 2 may be younger and closer than previously thought. However, G284.2642−00.3156 may have been formed subsequent to the formation of Westerlund 2 as a result of triggered star formation in surrounding molecular clouds (Deharveng et al. 2005; Oey et al. 2005). Further studies will determine whether this star is a cluster member or a result of triggered star formation, as well as the distance to this cluster. High-resolution spectra of both the O4 star and Westerlund 2 would allow a measurement of their relative radial velocities and would help establish whether this star is a cluster member.

6. CONCLUSION

We found 33 stars that exhibited a mid-IR excess above photospheric levels in the field surrounding RCW 49. We combined our new spectral classifications with known literature classifications and optical, near, and mid-IR photometry to model the spectral energy distributions of 184 stars. Stars with mid-IR excesses span all spectral classes from B to early K. We modeled the excess for each star as a single-component blackbody and found that for the G18 stars the excess is consistent with a debris disk or some transitional phase between primordial circumstellar disk and debris disk. For these 18 stars the additional blackbody component was found to have fractional bolometric disk-to-star luminosity ratios, $L_{\rm IR}/L_*$, ranging from 10^{-3} to 10^{-2}, with temperatures ranging from 220 to 820 K. These temperatures and fractional disk-to-star luminosities are consistent with warm inner dust of debris disks, which could be analogous to asteroid-belt–type objects.

REFERENCES

Aumann, H. H., & Probst, R. G. 1991, ApJ, 368, 264
Aumann, H. H., et al. 1984, ApJ, 278, L23
Backman, D. E., Gillett, F. C., & Witteborn, F. C. 1992, ApJ, 385, 670
Backman, D. E., & Paresce, F. 1993, in Protostars and Planets III, ed. E. Levy & J. I. Lunine (Tucson: Univ. Arizona Press), 1253
Benjamin, R., et al. 2003, PASP, 115, 953
Burgasser, A., et al. 2000, ApJ, 531, L57
Burrows, A., Hubbard, W. B., Lunine, J. I., & Liebert, J. 2001, Rev. Mod. Phys., 73, 719
Carraro, G., & Munari, U. 2004, MNRAS, 347, 625
Chen, C. H., & Jura, M. 2001, ApJ, 560, L171
Churchwell, E. B., et al. 2004, ApJS, 154, 322
Cohen, M., Megeath, S. T., Hammersley, P. L. Martín-Luis, F., & Stauffer, J. 2003, AJ, 125, 2645
Deharveng, L., Zavagno, A., & Caplan, J. 2005, A&A, 433, 565
De Jager, C., & Nieuwenhuijzen, H. 1987, A&A, 177, 217
Evans, H. J., et al. 2003, PASP, 115, 965
Fazio, G., et al. 2004, ApJS, 154, 10
Gillett, F. 1986, in Light on Dark Matter, ed. F. P. Israel (Doedrecht: Reidel)
Hatzes, A., et al. 2000, ApJ, 544, L145
Herbig, G. H. 1995, ARA&A, 33, 19
Indebetouw, R., et al. 2005, ApJ, 619, 931
Johnson, H. L. 1966, ARA&A, 4, 193
Kessler-Silacci, J. E., Hillenbrand, L. A., Blake, G. A., & Meyer, M. R. 2005, ApJ, 622, 404

Kurucz, R. 1993, Kurucz CD-ROM 13, ATLAS 9 Stellar Atmospheres Programs and 2 km/s Grid (Cambridge: SAO)
Lagrange, A.-M., Backman, D. E., & Artymowicz, P. 2000, in Protostars and Planets IV, ed. V. Mannings, A. P. Boss, & S. S. Russell (Tucson: Univ. Arizona Press), 639
Li, A., & Draine, B. T. 2001, ApJ, 554, 778
Mercer, E. P., et al. 2004, ApJS, 154, 328
Meyer M. R., & Beckwith S. V. W. 2000, in *ISO* Survey of a Dusty Universe, ed. D. Lemke et al. (Berlin: Springer), 341
Meyer M. R., et al. 2001, in The Origins of Stars and Planets: The VLT View, ed. J. Alves & M. McCaughrean (Berlin: Springer), 463
Meynet, G., Maeder, A., Schaller, G., Schaerer, D., & Charbonnel, C. 1994, A&AS, 103, 97
Moffat, A. F. J, Shara, M. M., & Potter, M. 1991, AJ, 102, 642
Oey, M. S., Watson, A. M., Kern, K., & Walth, G. L. 2005, AJ, 129, 393
Schmidt-Kaler, Th. 1982, in Numerical Data and Functional Relationships in Science and Technology, ed. K. Schaifers & H. H. Voigt (Berlin: Springer)
Shara, M. M., Moffat, A. F. J., Smith, L. F., & Potter, M. 1991, AJ, 102, 716
Smith, B. A., & Terrile, R. J 1984, Science, 226, 1421
Walborn, N. R., & Fitzpatrick, E. L. 1990, PASP, 102, 379
Whitney, B. A., et al. 2004, ApJS, 154, 315
Yamashita, Y., Nariai, K., & Norimoto, Y. 1976, An Atlas of Representative Stellar Spectra (New York: Wiley)